Adaptive Extended Kalman Filter Based Fusion Approach for High Precision UAV Positioning in Extremely Confined Environments

Beiya Yang, *Graduate Student Member, IEEE*, Erfu Yang, *Senior Member, IEEE*, Leijian Yu, and Cong Niu, *Member, IEEE*

***Abstract*—For unmanned aerial vehicle (UAV) based smart inspection in extremely confined environments, it is impossible for precise UAV positioning with global positioning system (GPS), owing to the satellite signal block. Therefore, the ultra-wideband (UWB) based technology has attracted extensive attention under such circumstances. However, due to the unpredictable propagation condition and the time-varying operational environment, the localisation performance oscillation caused by the changing measurement noise may lead to the instability of UAV. To mitigate the effects, in this paper, a high precision UAV positioning system which integrates the inertial measurement unit (IMU) and UWB with the adaptive extended Kalman filter (AEKF) is proposed. Compared with the traditional EKF based approach, the estimated and recorded information from previous processes is exploited to adaptively estimate and further control the estimation of the noise covariance matrices for performance improvement. Finally, simulations and experiments have been conducted in extremely confined environments. According to the results, the proposed algorithm can significantly improve the position update rate, the median positioning error, the 95^{th} percentile positioning error and the average standard deviation (STD) into 88Hz, 0.102m, 0.192m and 0.052m, which is applicable for applications in focused environments.**

***Index Terms*—Unmanned aerial vehicle (UAV), adaptive extended Kalman filter (AEKF), ultra-wideband (UWB), inertial measurement unit (IMU), sensor fusion, extremely confined environments.**

I. Introduction

FOR unmanned aerial vehicle (UAV) applications in the smart inspection area, such as the inspection inside the industrial boiler, penstocks, tubes, the small oil pressure vessel or water tank [1], [2], known as extremely confined environments [3], [4], how to acquire the precise UAV position information becomes a much-sought research challenge, due to the satellite signal block in such environments [5], [6].

The researches and investigations on plenty of existing localisation technologies have already been conducted, considering potential applications on UAV positioning. Within these, the visual odometry (VO) is the extensively utilised method, due to the centimetre-level accuracy and low prior information requirement features [7]. However, the low visibility condition in such environments will greatly affect the accuracy and the reliability [8]. Alternatively, the inertial navigation system (INS) or inertial measurement unit (IMU) based positioning technology is the other widely used positioning technology. But, considering the accuracy degradation caused by the error accumulation, it often serves as part of the sensor fusion approach for precise UAV positioning. Furthermore, light detection and ranging (LiDAR) [9] and ultrasonic [10] based localisation technologies have also attracted lots of attention in this area, due to the enhanced positioning accuracy. Yet, the critical issues including the extremely high system cost, weight and energy consumption for LiDAR, limited localisation coverage and vulnerable to the unpredictable signal occlusion for ultrasonic will restrict their applications on UAV positioning [11]. To overcome aforementioned issues, the ultra-wideband (UWB) based localisation technology becomes an ideal candidate, due to the centimetre-level ranging accuracy and reliable performance in different environments. Meanwhile, owing to the essential characteristics of the electromagnetic wave, the low visibility condition, feature-less issue and error accumulation can be ignored with the UWB based localisation technology [7], [12].

Nevertheless, the restriction still exists for the UWB based localisation technology which limits its applications on UAV in such environments. Owing to the inherent properties of the radio frequency (RF) signal, the additional propagation delay and changing measurement noise caused by the unpredictable propagation condition and the time-varying operational environment always exist which will lead to the localisation performance oscillation and may result in the instability of UAV. Under such circumstances, plenty of researches have been carried out. Among them, the sensor fusion based approach with the integration of IMU and UWB is known as the one extensively exploited on UAV positioning, owing to the implementation simplicity and sufficient accuracy. In [13], an IMU, UWB and vision-based sensor fusion approach was proposed for the decimetre-level accuracy localisation of mini-UAV in the indoor environment. Similarly, Guo et al. [14] developed a UAV positioning system with the integration of IMU and UWB through extended Kalman filter (EKF). But differently, the calibration and outlier detection methods were added to filter the unreasonable value for the distance information, to prevent the performance oscillation. Li et al. [15] also focused

This article is fully supported by Research Excellence Award studentship from University of Strathclyde and partially supported by Low Cost Intelligent UAV Swarming Technology for Visual Inspection project from the UK Net Zero Technology Centre (Grant No. AI-P-028) and the MOEA/D-PPR research project (Grant No.: IEC-NSFC-211434) funded by the Royal Society. Corresponding author: Erfu Yang.

The authors are within the Department of Design, Manufacturing and Engineering Management, University of Strathclyde, 75 Montrose Street, Glasgow G1 1XJ, UK (email: beiya.yang@strath.ac.uk, erfu.yang@strath.ac.uk, leijian.yu@strath.ac.uk, cong.niu@strath.ac.uk)

This is a peer reviewed, accepted author manuscript of the following research article: Yang, B., Yang, E., Yu, L., & Niu, C. (2022). Adaptive extended Kalman filter based fusion approach for high precision UAV positioning in extremely confined environments. IEEE/ASME Transactions on Mechatronics. https://doi.org/10.1109/TMECH.2022.3203875

on the same research direction. The EKF based sensor fusion approach was utilised to reduce the localisation latency and improve the accuracy for micro aerial vehicles (MAVs). To improve the performance of the existing approaches, different researches have been carried out. Feng et al. [16] proposed an IMU and UWB based Kalman filter approach for the positioning and navigation of mobile robot. The geometric distribution of fixed anchor nodes was analysed for performance improvement, and the additional measured angle information between anchor node and the tag node on the robot was exploited to further reduce deployment cost of anchor nodes. The angular rate was introduced by Strohmeier et al. [17] in the state prediction process to deal with the potential drift for the orientation information from IMU. However, instead of the ranging information, the estimated position information from UWB was exploited as the observation information for correction, which means that the performance of this approach will be greatly influenced by the accuracy and reliability of the position information from UWB. Similarly, the angular rate was also considered in the process model by authors in [18]. But differently, the ranging information was directly served as the observation information for correction. Meanwhile, the distance calibration and outlier detection methods were also taken into account to filter the distance measurements for performance improvement. However, the number of the reference points will restrict the calibration and the system performance.

One critical issue still exists which restrict the performance of the aforementioned approaches is the requirement of the prior information. The accuracy for the prior information, including the process and measurement noise covariance matrices, highly affects the performance of the EKF based sensor fusion approach [19]. Inappropriate value can cause the sharp performance degradation, even the filtering divergence [20]. For the IMU and UWB based UAV positioning, since the propagation condition and operational environment are unpredictable and time-varying during the flight of UAV, the performance oscillation or degradation may appear, with the constant and inaccurate noise covariance matrices for the traditional EKF based sensor fusion approaches [21]. To remedy the existing problem and provide accurate noise covariance matrices for performance improvement, the adaptive extended Kalman filter (AEKF) is known as the most effective method [19], [22].

To solve the above mentioned issue for high performance UAV positioning, a high precision UAV positioning system is proposed which leverages the integration of IMU and UWB based AEKF approach for UAV positioning, focusing on smart inspection applications in extremely confined environments. Main contributions of this article are listed as follow:

1) An AEKF based UAV positioning approach is proposed, focusing on the robust and high precision localisation. With the adaptively estimated noise covariance matrices and the additional weighting factors, the proposed approach can significantly improve the UAV localisation performance and the stability in extremely confined environments.
2) An IMU and UWB based UAV positioning system is designed and developed for the validation and demonstration of the proposed algorithm. Compared with the conventional maximum likelihood estimation (MLE) based two-way time of flight (TW-TOF) localisation algorithm and the state-of-the-art sensor fusion based approaches, the proposed approach can significantly improve the UAV localisation performance and the stability in focused environments.

The rest of the paper is organised as follows. Section II gives an introduction about the conventional UWB based UAV positioning approach, including the TW-TOF based ranging protocol and the MLE based localisation method. Afterwards, Section III provides a detailed description for the IMU and UWB based sensor fusion approach, including the coordinate system transformation, the overview for the traditional EKF based approach and the description for the proposed algorithm. To validate the effectiveness, in Section IV, the simulations and experiments for all the aforementioned algorithms are carried out and analysed. Finally, the conclusion is drawn in Section V.

II. UWB BASED UAV POSITIONING

This section mainly describes the localisation scheme for the conventional localisation approach of the UWB based localisation system with the TW-TOF ranging scheme on UAV positioning.

A. TW-TOF based ranging protocol

Considering the existing characteristics of the TW-TOF based ranging protocol including high accuracy, low computational complexity, implementation simplicity and no requirement for the strict clock synchronisation between sensor nodes, the localisation approach based on TW-TOF has already become the most commonly utilised approach for RF based localisation system, especially for the UWB based system on UAV positioning [23]–[26]. With the measured time of departure (TOD) (l_{U1}, l_{A2}) and time of arrival (TOA) (l_{U2}, l_{A1}), the clock difference between tag and anchor node can be cancelled directly. No strict clock synchronisation between these nodes is required. Afterwards, throughout the arithmetic theory of TW-TOF, the distance between these two sensor nodes can be expressed as

$$d_i = [(l_{U2} - l_{U1}) - (l_{A2} - l_{A1})]c/2, \tag{1}$$

where, d_i represents the measured distance between UAV and anchor node i ($i = 1, 2, ..., n$), c is the velocity of the electromagnetic wave.

Here, the MLE based method is adopted to calculate the position information of UAV with the measured distance [26].

B. Maximum likelihood estimation based localisation approach

In the actual process, the measurement noise always exists at each sensor node which can be represented as

$$d_{AD}(t) = \tilde{d}_{AD}(t) + \gamma(t), \tag{2}$$

where, $\tilde{d}_{AD}(t)$ is supposed as the true value of the distance between two sensor nodes, the measurement noise of the measured distance which comes from UWB sensor nodes is assumed as $\gamma(t)$. Here the measurement noise is modelled as the additive white Gaussian noise (AWGN) with zero mean and $\boldsymbol{Q}_\gamma$ covariance.

Thus, according to the arithmetic theory of the multilateration, following equations can be derived

$$\begin{cases} d_1(t) = \|\boldsymbol{p} - \boldsymbol{p}_1\| + \gamma_1(t) \\ d_2(t) = \|\boldsymbol{p} - \boldsymbol{p}_2\| + \gamma_2(t) \\ \vdots \\ d_n(t) = \|\boldsymbol{p} - \boldsymbol{p}_n\| + \gamma_n(t) \end{cases}. \tag{3}$$

Among above equations, $\boldsymbol{p} = [x, y, z]^T$ and $\boldsymbol{p}_i = [x_i, y_i, z_i]^T$ are supposed as the position information of the UAV and anchor node i, respectively. Afterwards, transforming these equations into matrix form

$$\boldsymbol{D} = f(\boldsymbol{p}) + \boldsymbol{\Gamma}, \tag{4}$$

where, $\boldsymbol{D}$ is assumed as the measured distance matrix from UWB sensor nodes, $f(\boldsymbol{p})$ represents the actual distance matrix and $\boldsymbol{\Gamma}$ is supposed as the measurement noise matrix which can be written as follow

$$\boldsymbol{D} = [d_1(t), d_2(t), ..., d_n(t)]^T, \tag{5}$$

$$f(\boldsymbol{p}) = [\|\boldsymbol{p} - \boldsymbol{p}_1\|, \|\boldsymbol{p} - \boldsymbol{p}_2\|, ..., \|\boldsymbol{p} - \boldsymbol{p}_n\|]^T, \tag{6}$$

$$\boldsymbol{\Gamma} = [\gamma_1(t), \gamma_2(t), ..., \gamma_n(t)]^T. \tag{7}$$

Accordingly, the likelihood function can be derived

$$\begin{aligned} p(\boldsymbol{D}, \boldsymbol{p}) = & \frac{1}{(2\pi)^{\frac{n}{2}} det(\boldsymbol{Q}_\gamma)^{\frac{1}{2}}} \\ & \cdot exp[-\frac{1}{2}(\boldsymbol{D} - f(\boldsymbol{p}))^T \boldsymbol{Q}_\gamma^{-1}(\boldsymbol{D} - f(\boldsymbol{p}))] \end{aligned}. \tag{8}$$

Finally, the UAV position information can be attained through the estimation. However, considering the unpredictable propagation condition and the time-varying operational environment, the measurement noise is varying all the time which may result in the huge oscillation of the localisation performance. For traditional applications like the personal or package tracking, this oscillation can be ignored directly, owing to the short-term feature. But for applications on UAV positioning, the situation is changed. Even a short-term positioning drift can result in the instability of UAV, especially in focused application scenarios [12]. Consequently, eliminating and filtering the performance oscillation will be a special challenge for UAV applications.

III. IMU AND UWB BASED SENSOR FUSION

In order to remedy the aforementioned issue, to achieve a high precision UAV positioning for the stable control of it inside the extremely confined space, the IMU and UWB based sensor fusion method will be introduced in this section.

A. Transformation of the coordinate system

In order to appropriately describe the motion of UAV, a suitable coordinate system is required. For traditional applications of UAV, the global navigation coordinate system is often set to be north-east-down (NED) coordinate system, then convert the position information from NED to the body frame of UAV for position control. However, for our applications, the local navigation coordinate system can be directly determined by UWB anchor nodes. Therefore, the conversion for the acceleration from IMU in its coordinate system to the local navigation frame established by UWB anchor nodes is sufficient.

In the system, the IMU is attached on the UWB tag node which is determined as the right-handed coordinate system as shown in Fig. 5. Here, the coordinate system of IMU is set to be $OX_{IMU}Y_{IMU}Z_{IMU}$, and the local navigation coordinate system is assumed as $OX_LY_LZ_L$. For the purpose of preventing the gimbal lock problem, the quaternion method has already become the most widely utilised approach to represent the orientation and rotation for UAV applications, compared with Euler angle method. However, in order to make the transformation process more intuitive, the Euler angle method is leveraged here to clearly demonstrate the whole transformation process. Here, the three angles between the local navigation frame and IMU frame, estimated by the IMU, including the Roll, Pitch and Yaw is defined as ϕ, θ and ψ. Thus, the coversion equation from IMU frame to the local navigation frame can be derived

$$\boldsymbol{a}^L = \boldsymbol{C}_{YL}\boldsymbol{C}_{PY}\boldsymbol{C}_{IP}\boldsymbol{a}^{IMU}, \tag{9}$$

where, $\boldsymbol{C}_{IP}$, $\boldsymbol{C}_{PY}$ and $\boldsymbol{C}_{YL}$ represent the transformation matrix between the IMU/Pitch frame, the Pitch/Yaw frame and the Yaw/Local frame,

$$\boldsymbol{C}_{IP} = \begin{bmatrix} 1 & 0 & 0 \\ 0 & \cos\phi & -\sin\phi \\ 0 & \sin\phi & \cos\phi \end{bmatrix}, \tag{10}$$

$$\boldsymbol{C}_{PY} = \begin{bmatrix} \cos\theta & 0 & \sin\theta \\ 0 & 1 & 0 \\ -\sin\theta & 0 & \cos\theta \end{bmatrix}, \tag{11}$$

$$\boldsymbol{C}_{YL} = \begin{bmatrix} \cos\psi & -\sin\psi & 0 \\ \sin\psi & \cos\psi & 0 \\ 0 & 0 & 1 \end{bmatrix}. \tag{12}$$

$\boldsymbol{a}^L$ and $\boldsymbol{a}^{IMU}$ denote the acceleration in local navigation frame and IMU frame. If the gravitational acceleration g is not removed in the local navigation frame, then the equation should be re-derived as

$$\boldsymbol{a}^L = \boldsymbol{C}_{YL}\boldsymbol{C}_{PY}\boldsymbol{C}_{IP}\boldsymbol{a}^{IMU} + \begin{bmatrix} 0 \\ 0 \\ g \end{bmatrix}. \tag{13}$$

B. EKF based sensor fusion approach

According to the kinematic model, the state transition or prediction equation can be expressed as

$$\begin{cases} \hat{\boldsymbol{p}}_{k/k-1} = \boldsymbol{p}_{k-1} + \Delta T \boldsymbol{v}_{k-1} + \frac{\Delta T^2}{2}\boldsymbol{a}_{k-1}^L \\ \hat{\boldsymbol{v}}_{k/k-1} = \boldsymbol{v}_{k-1} + \Delta T \boldsymbol{a}_{k-1}^L \end{cases}. \tag{14}$$

Within the equation, the UAV position information $\boldsymbol{p} = [x, y, z]^T$ and the UAV velocity $\boldsymbol{v} = [v_x, v_y, v_z]^T$ in each direction are the state information to be estimated. ΔT denotes the time interval between two measurements of IMU and $\boldsymbol{a}^L = [a_x^L, a_y^L, a_z^L]^T$ represents the measured and converted acceleration of UAV in local navigation frame all are the input variables. Considering the existing bias $\boldsymbol{b}_a$ and the measurement noise $\boldsymbol{\omega}$ for the accelerometer from the IMU, the true value for the acceleration can be represented as

$$\tilde{\boldsymbol{a}}^L = \boldsymbol{a}^L - \boldsymbol{b}_a - \boldsymbol{\omega}. \tag{15}$$

Corresponding to the literature in [18], [27], $\boldsymbol{b}_a$ is modelled as Gaussian random walk process with zero mean and $\boldsymbol{Q}_b$ covariance, $\boldsymbol{\omega}$ is modelled as AWGN with zero mean and $\boldsymbol{Q}_\omega$ covariance.

Then, transforming the equation into matrix form yields

$$\hat{\boldsymbol{u}}_{k/k-1} = \boldsymbol{F}_k \boldsymbol{u}_{k-1} + \boldsymbol{B}_k \boldsymbol{a}_{k-1}^L, \tag{16}$$

$$\hat{\boldsymbol{A}}_{k/k-1} = \boldsymbol{F}_k \boldsymbol{A}_{k-1} \boldsymbol{F}_k^T + \boldsymbol{Q}_k, \tag{17}$$

where, $\boldsymbol{u} = [x, v_x, y, v_y, z, v_z]^T$ is the state vector,

$$\boldsymbol{F}_k = \boldsymbol{I}_3 \otimes \begin{bmatrix} 1 & \Delta T \\ 0 & 1 \end{bmatrix} \tag{18}$$

represents the state transition matrix,

$$\boldsymbol{B}_k = \boldsymbol{I}_3 \otimes \begin{bmatrix} \frac{\Delta T^2}{2} \\ \Delta T \end{bmatrix} \tag{19}$$

is the control matrix, $\boldsymbol{I}_3$ denotes the 3×3 identity matrix, "$\otimes$" represents the Kronecker product, $\boldsymbol{A}$ represents the covariance matrix and

$$\boldsymbol{Q}_k = \boldsymbol{B}_k \boldsymbol{Q}_b \boldsymbol{B}_k^T + \boldsymbol{B}_k \boldsymbol{Q}_\omega \boldsymbol{B}_k^T \tag{20}$$

is the process noise covariance matrix determined by the bias and measurement noise from accelerometer.

With the same ranging protocol in Section II-A, the distance information between UAV and fixed anchor nodes is exploited to serve as the input measurement for correction process to eliminate the accumulation error from IMU.

Then the measurement model can be established as

$$\boldsymbol{\rho}_k = \boldsymbol{H}_k \hat{\boldsymbol{u}}_{k/k-1} + \boldsymbol{\gamma}_k, \tag{21}$$

where, $\boldsymbol{\rho}_k$ denotes the distance measurements matrix, $\boldsymbol{H}_k$ represents the observation transition matrix,

$$\boldsymbol{H}_k = \begin{bmatrix} \frac{\partial d_{1,k/k-1}}{\partial \hat{x}_{k/k-1}} & 0 & \frac{\partial d_{1,k/k-1}}{\partial \hat{y}_{k/k-1}} & 0 & \frac{\partial d_{1,k/k-1}}{\partial \hat{z}_{k/k-1}} & 0 \\ \frac{\partial d_{2,k/k-1}}{\partial \hat{x}_{k/k-1}} & 0 & \frac{\partial d_{2,k/k-1}}{\partial \hat{y}_{k/k-1}} & 0 & \frac{\partial d_{2,k/k-1}}{\partial \hat{z}_{k/k-1}} & 0 \\ \vdots & \vdots & \vdots & \vdots & \vdots & \vdots \\ \frac{\partial d_{n,k/k-1}}{\partial \hat{x}_{k/k-1}} & 0 & \frac{\partial d_{n,k/k-1}}{\partial \hat{y}_{k/k-1}} & 0 & \frac{\partial d_{n,k/k-1}}{\partial \hat{z}_{k/k-1}} & 0 \end{bmatrix}_{n \times 6}, \tag{22}$$

calculated by the first order Taylor expansion, the measurement noise $\boldsymbol{\gamma}$ from UWB sensor nodes is modelled as AWGN with zero mean and $\boldsymbol{Q}_\gamma$ covariance.

Finally, the Kalman gain can be calculated

$$\boldsymbol{K}_{KF} = \hat{\boldsymbol{A}}_{k/k-1} \boldsymbol{H}_k^T (\boldsymbol{H}_k \hat{\boldsymbol{A}}_{k/k-1} \boldsymbol{H}_k^T + \boldsymbol{R}_k)^{-1}, \tag{23}$$

where, $\boldsymbol{R}_k$ is the measurement noise covariance matrix determined by the measurement noise from UWB sensor nodes.

C. AEKF based sensor fusion approach

Even the unexpected performance oscillation can be eliminated by the EKF based sensor fusion approach. However, the unknown and constantly changing process noise covariance matrix $\boldsymbol{Q}_k$ and measurement noise covariance matrix $\boldsymbol{R}_k$ caused by the unpredictable propagation condition and the time-varying operational environment still have huge impact on the localisation performance. Therefore, the AEKF based sensor fusion approach will be investigated to adaptively estimate these noise covariance matrices for the stable and reliable UAV positioning under different circumstances [22], [28].

1) Estimation of the noise covariance matrices: Accordingly, the difference between the distance measurements and the predicted information can be calculated through the observation matrix and the estimated information from the state prediction process

$$\boldsymbol{\rho}'_k = \boldsymbol{\rho}_k - \boldsymbol{H}_k \hat{\boldsymbol{u}}_{k/k-1}, \tag{24}$$

where, $\boldsymbol{\rho}'_k$ represents the difference between the observation measurements and the predicted value. Thus, the innovation covariance matrix $\hat{\boldsymbol{C}}_{\boldsymbol{\rho}'_k}$ can be derived

$$\hat{\boldsymbol{C}}_{\boldsymbol{\rho}'_k} = \frac{1}{M} \sum_{i=k-M+1}^{k} \boldsymbol{\rho}'_i {\boldsymbol{\rho}'_i}^T, \tag{25}$$

where, M represents the window size or sampling number, which has the great impact on the estimation accuracy and stability. If a smaller M is selected, the computational complexity of the algorithm can be reduced, and the estimation process can be more adaptive to catch up the changes in the current process. However, the estimation process will become noisy and may lead to the filtering divergence. On the contrary, a larger M can improve the stability of the estimation process, which means a much smoother result. Nevertheless, the computational complexity will be increased, and the larger M may cause the adaptation ability lose of the algorithm. Considering all the existing issues, the M in the simulations and experiments is set as 10 through trial and error.

Then, the measurement noise covariance matrix $\boldsymbol{R}_k$ can be obtained

$$\boldsymbol{R}_k = \hat{\boldsymbol{C}}_{\boldsymbol{\rho}'_k} - \boldsymbol{H}_k \hat{\boldsymbol{A}}_k \boldsymbol{H}_k^T. \tag{26}$$

On the other hand, from (15), (16) and (23), the state prediction noise at k round can be approximated as

$$\begin{aligned} \boldsymbol{B}_k \boldsymbol{b}_{ak} + \boldsymbol{B}_k \boldsymbol{\omega}_k &= \hat{\boldsymbol{u}}_k - \hat{\boldsymbol{u}}_{k/k-1} \\ &= \boldsymbol{K}_{KF} (\boldsymbol{\rho}_k - \boldsymbol{H}_k \hat{\boldsymbol{u}}_{k/k-1}). \end{aligned} \tag{27}$$

Therefore, the process noise covariance matrix $\boldsymbol{Q}_k$ can be derived as

$$\begin{aligned} \boldsymbol{Q}_k &= \boldsymbol{K}_{KF} E[\boldsymbol{\rho}'_k {\boldsymbol{\rho}'_k}^T] \boldsymbol{K}_{KF}^T \\ &= \boldsymbol{K}_{KF} \hat{\boldsymbol{C}}_{\boldsymbol{\rho}'_k} \boldsymbol{K}_{KF}^T \end{aligned}. \tag{28}$$

With the estimated process noise covariance matrix $\boldsymbol{Q}_k$ and measurement noise covariance matrix $\boldsymbol{R}_k$, the localisation performance can be further improved. However, the changing process and measurement noise caused by the unpredictable

propagation condition, operational environment and the varying time interval between two rounds acceleration measurements still may lead to the inaccurate estimation of these two noise covariance matrices, which will result in the localisation performance oscillation, even the filtering divergence.

2) Estimation of weighting factors: In order to remedy the above mentioned issue, two different weighting factors α and β, and the offline data $\boldsymbol{R}_{offline}$ and $\boldsymbol{Q}_{offline}$ will be introduced [28]. Here, $\boldsymbol{R}_{offline}$ and $\boldsymbol{Q}_{offline}$ are calculated through the captured offline data from sensor nodes (UWB sensor nodes and IMU) with UAV statically at the original position before the flight of it.

Firstly, for the estimation of the measurement noise covariance matrix, a weighting factor α is introduced to eliminate the influence of the varying measurement noise from UWB sensor nodes.

$$\boldsymbol{R}'_k = (1-\alpha)\boldsymbol{R}_{offline} + \alpha \boldsymbol{R}_k. \tag{29}$$

As shown in the above equation, the weighting factor α is added into the estimation process. $\boldsymbol{R}'_k$ is the estimated measurement noise covariance matrix limited by the additional weighting factor. α is set within $0\leq\ \alpha\ \leq 0.5$ to prevent the filtering divergence caused by the unexpected oscillation of the current measurements. Clearly, with the increasing of α, the estimation of $\boldsymbol{R}'_k$ will more rely on the current measurements, which means the oscillation of $\boldsymbol{R}'_k$, but the system can react fast. However, the performance oscillation may occur and cause the divergence. On the contrary, the performance oscillation will be eased with a more stable estimation of $\boldsymbol{R}'_k$, but the system will take more time to catch up the changes.

To adaptively estimate the weighting factor α, the current difference between the observation measurements and the predicted value $\boldsymbol{\rho}'_k$, and average difference $\rho'_{initial}$ from the previous processes will be utilised. Where $\rho'_{initial}$ is calculated through the recorded estimation results from the state prediction process and the correction process with UAV statically at fixed points before the flight of it. Throughout these, α can be adaptively estimated as

$$\alpha_{adaptive} = \frac{\frac{1}{n}\sum_{i=1}^{n}[\boldsymbol{\rho}'_k]_{i1}}{\rho'_{initial}}\alpha_{initial}. \tag{30}$$

In which, n represents the number of anchor nodes in the system, and the initial guess $\alpha_{initial}$ is set to be 0.5. Clearly, with the augment of $\boldsymbol{\rho}'_k$, $\alpha_{adaptive}$ will become larger, and the estimation of $\boldsymbol{R}'_k$ will more rely on the current measurements to catch up the changes. On the contrary, with smaller difference, the estimation of $\boldsymbol{R}'_k$ will give more credence on the previous measurements, which means a more stable value.

On the other hand, to prevent the performance oscillation and potential filtering divergence, another weighting factor β is introduced and adaptively estimated through the recorded average time interval $\Delta T_{average}$ between two rounds IMU acceleration measurements with UAV statically at fixed points, before the operation of the localisation system.

$$\boldsymbol{Q}'_k = (1-\beta)\boldsymbol{Q}_{offline} + \beta \boldsymbol{Q}_k, \tag{31}$$

$$\beta_{adaptive} = \frac{\Delta T}{\Delta T_{average}}\beta_{initial}. \tag{32}$$

Similar to α, the weighting factor β is also set within $0\leq\ \beta\ \leq 0.5$ to prevent the filtering divergence, and the initial guess $\beta_{initial}$ is given as 0.5. Throughout the estimation process, with a larger ΔT, the estimation of $\boldsymbol{Q}'_k$ will more rely on the current measurements to catch up the changes. By contrast, the result can be smoother, but the performance degradation is inevitable. Moreover, since $\boldsymbol{R}_k$ is calculated through two positive definite matrices as from (26), which may lead to a negative estimation and cause the filtering divergence. Therefore, in the estimation process, if a negative estimation of $\boldsymbol{R}_k$ is detected, α in this round will be directly set to zero to prevent the potential filtering divergence.

Finally, with the estimated $\boldsymbol{Q}'_k$ and $\boldsymbol{R}'_k$, the localisation result can be further updated.

IV. Simulation and Experiment

In this section, cases of simulations and experiments have been carried out to validate the effectiveness of the proposed algorithm on UAV positioning.

A. Simulation

Considering the safety reason for flying UAV in the extremely confined environment and to prove the effectiveness of the proposed algorithm before actual experiments, simulations have been carried out in Gazebo environment [29]. In the simulation, the UAV is placed in a confined space (1.95m $\times$ 3.0m $\times$ 2.3m) with four anchor nodes mounted on X-Z plane. This is to simulate the actual application that all anchor nodes can only be deployed near the entrance of such space, due to the inaccessible and extremely confined features for focused environments. The coordinates of each anchor node and the simulation environment are depicted in Fig. 1. In the simulation, the UAV is set to fly along a reverse "S" trajectory, the ground truth for the position information of UAV is directly obtained from the simulation environment. The simulations for different algorithms, including the conventional MLE based TW-TOF, the EKF based sensor fusion algorithm in this paper, the EKF based approach with the distance filter proposed by Guo et al. [14], the sensor fusion based approach presented in [17], the UWB and IMU based localisation approach designed by Li et al. [18] and the AEKF based algorithm with different weighting factors have been compared with the proposed algorithm. In order to exhaustively validate the effectiveness of the proposed algorithm, two simulations under different measurement noise of the acceleration and distance information have been carried out. In the first simulation, the standard deviation (STD) for the measurement noise of the simulated acceleration and distance information are assumed as constant and set to be 0.5m/s^2 and 0.1m. In the second simulation, the STD for these two measurement noises is randomly set within [0,0.5]m/s^2 and [0,0.2]m to simulate the variation of the operational environment.

As depicted in Fig. 2, the localisation performance for these algorithms in the first simulation has been demonstrated

TABLE I
PERFORMANCE ANALYSIS FOR THE SIMULATION RESULTS

Simulation Number	Algorithm	Median Error	Improved	95^{th} Error	Improved	Average STD	Improved
Simulation 1	MLE based TW-TOF	0.148m	N/A	0.271m	N/A	0.067m	N/A
–	EKF In This Paper	0.087m	41.2%	0.235m	13.3%	0.069m	-3.0%
–	[14]	0.085m	42.6%	0.202m	25.5%	0.058m	13.4%
–	[17]	0.057m	61.4%	0.157m	42.1%	0.042m	37.3%
–	[18]	0.070m	52.7%	0.145m	46.5%	0.036m	46.3%
–	AEKF ($\alpha = \beta = 0.3$)	**0.041m**	**72.3%**	0.133m	50.9%	0.035m	47.8%
–	AEKF ($\alpha = \beta = 0.5$)	0.048m	67.6%	0.149m	45.0%	0.042m	37.3%
–	**Our Proposed**	0.042m	71.6%	**0.117m**	**56.8%**	**0.031m**	**53.7%**
Simulation 2	MLE based TW-TOF	0.129m	N/A	0.381m	N/A	0.116m	N/A
–	EKF In This Paper	0.077m	40.3%	0.226m	40.7%	0.064m	44.8%
–	[14]	0.088m	31.8%	0.258m	32.3%	0.079m	31.9%
–	[17]	0.066m	48.8%	0.143m	62.5%	0.042m	63.8%
–	[18]	0.082m	36.4%	0.167m	56.2%	0.050m	56.9%
–	AEKF ($\alpha = \beta = 0.3$)	**0.052m**	**59.7%**	0.149m	60.9%	0.042m	63.8%
–	AEKF ($\alpha = \beta = 0.5$)	0.060m	53.5%	**0.141m**	**63.0%**	0.042m	63.8%
–	**Our Proposed**	**0.052m**	**59.7%**	0.142m	62.7%	**0.041m**	**64.7%**

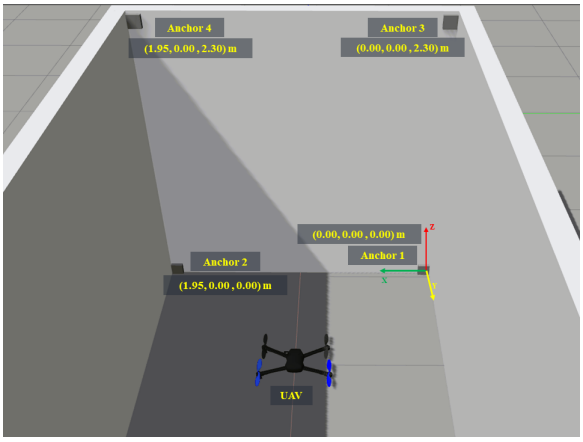

Fig. 1. Simulation environment.

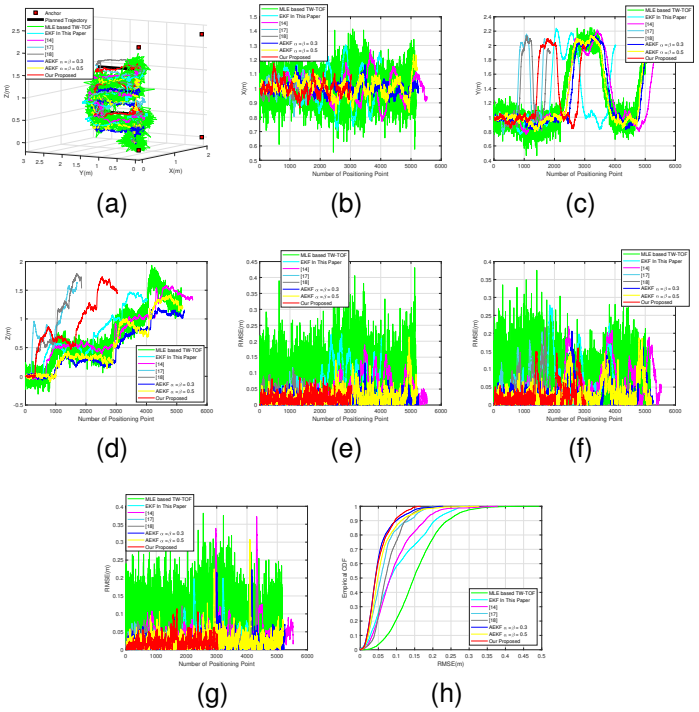

Fig. 2. Flight test results in the first simulation. (a) 3D trajectories for different algorithms. (b) 3D trajectories in X direction. (c) 3D trajectories in Y direction. (d) 3D trajectories in Z direction. (e) RMSE (m) in X direction. (f) RMSE (m) in Y direction. (g) RMSE (m) in Z direction. (h) eCDF for different algorithms.

through different perspectives, including the positioning trajectory, the trajectory in each direction, the positioning root mean square error (RMSE) in each direction and the empirical cumulative distribution function (eCDF) for these algorithms.

Firstly, when being focused on the positioning trajectory results in the first four figures, it can be observed that, the conventional MLE based TW-TOF algorithm holds the biggest oscillation in every direction due to the unreasonable value from the UWB sensor nodes. However, for all other sensor fusion based approaches, the trajectory results are significantly smoothed and improved. Meanwhile, in order to quantitatively assess the localisation performance of each algorithm, the RMSE for these algorithms in each direction plus with the eCDF and the detailed localisation error of each are illustrated in Fig. 2(e-h) and Table I. Specifically, from the RMSE simulation results, the same conclusion can be made. With the utilisation of the sensor fusion based approaches, the absolute accuracy and precision of the system are all improved significantly. For the approaches with the distance calibration and outlier detection methods in [14] and [18], when with the constant measurement noise STD, the performance is greatly improved with the average STD to be 0.058m and 0.036m. On the other hand, for the AEKF approaches, compared with the EKF in this paper and the three algorithms in [14], [17] and [18], with the estimated noise covariance matrices, the localisation performance is greatly improved with the median error, 95^{th} percentile error and average STD around 0.044m, 0.133m and 0.036m, respectively. When doing the comparison within the AEKF approaches, it can be observed that, the larger weighting factors lead to the larger performance oscillation. This is caused by the constant noise model in the first simulation. As aforementioned in Section III-C2 with

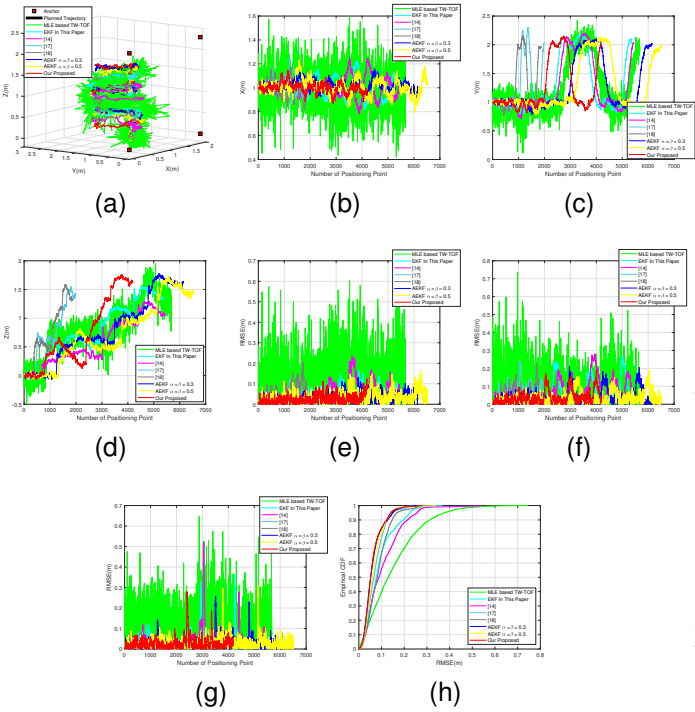

Fig. 3. Flight test results in the second simulation. (a) 3D trajectories for different algorithms. (b) 3D trajectories in X direction. (c) 3D trajectories in Y direction. (d) 3D trajectories in Z direction. (e) RMSE (m) in X direction. (f) RMSE (m) in Y direction. (g) RMSE (m) in Z direction. (h) eCDF for different algorithms.

a larger α and β, the estimation of $\boldsymbol{R}'_k$ and $\boldsymbol{Q}'_k$ will more rely on the current measurements, which means more changes on the estimation value of $\boldsymbol{R}'_k$ and $\boldsymbol{Q}'_k$. Therefore, with the relatively stable measurement noise model, larger weighting factors will lead to the performance oscillation, which means the drop-off for the precision of the algorithm. Finally, when being focused on the proposed AEKF algorithm, obviously, with the estimated weighting factors, the proposed AEKF algorithm holds the high performance with 0.042m median error, 0.117m 95^{th} percentile error and 0.031m average STD of the localisation error. Compared with the conventional MLE based TW-TOF algorithm, the performance is improved by 71.6%, 56.8% and 53.7%, respectively.

In order to comprehensively validate the performance of the proposed algorithm in the simulation environment, in the second simulation, the STD of these two measurement noises is randomly set within certain range. This is to simulate the variation of the operational environment. Same as the first simulation, the localisation performance for these algorithms in the second simulation has been demonstrated through different perspectives in Fig. 3 and summarised in Table I. Clearly, with the sensor fusion based algorithms, the localisation results are able to be greatly smoothed and improved. On the other hand, when being focused on the comparison between the AEKF based approaches and all other sensor fusion based approaches, a greatly performance improvement can be observed with AEKF approaches. This is because that the noise covariance matrices are adjusted manually and keep constant within the estimation process for all other sensor fusion based approaches, thus, when with the changing measurement noise model, the localisation performance can be significantly influenced. Meanwhile, for the two algorithms with the distance calibration and outlier detection methods in [14] and [18], the performance oscillation can be observed with the average STD dropped to 0.079m and 0.050m. This is also caused by the unsuitable calibration parameter leaded by the changing measurement noise model. Furthermore, different from the first simulation, the localisation performance for the AEKF algorithm with larger weighting factors is improved. With larger weighting factors, more trust is given to the current measurement, which means that the offline data has less influence on the localisation performance, the estimated noise covariance matrices are much more accurate. Considering the measurement noise model is keep changing in the current simulation, the localisation performance can be improved with more accurate noise covariance matrices, especially for the 95^{th} percentile error. Thus, larger weighting factors are more suitable for applications in the unstable operational environment. In additional, compared with all the other algorithms, the proposed AEKF algorithm still holds the high performance with 0.052m median error, 0.142m 95^{th} percentile error and 0.041m average STD of the localisation error. It should be declared that even the proposed algorithm has not held the best performance within all these three indexes, but it always shows the capability for high accuracy and precision localisation under different circumstances of the measurement noise.

TABLE II
THE PROBABILITY FOR FILTERING DIVERGENCE

AEKF Algorithms	Simulation 1	Simulation 2
$\alpha = \beta = 0.1$	0%	0%
$\alpha = \beta = 0.3$	0%	0%
$\alpha = \beta = 0.5$	0%	5%
$\alpha = \beta = 0.7$	40%	50%
$\alpha = \beta = 0.9$	90%	95%
Our Proposed	0%	0%

Moreover, rule out of the accuracy and precision of the algorithm, for UAV applications, the stability of the algorithm also needs to be considered. The filtering divergence for the proposed algorithm is more likely to happen with the keep changing noise covariance matrices, which may cause the position lost of UAV. For the purpose of verifying the stability of the proposed AEKF algorithm, the additional tests have been conducted. Two different simulations have been carried out with the constant and changing measurement noise model same as the previous simulations. Here the AEKF algorithms with different weighting factors (0.1, 0.3, 0.5, 0.7 and 0.9) and the proposed AEKF algorithm have been tested. Each algorithm has been tested 20 times with the same path in the previous simulations. The probability of each algorithm for filtering divergence in two simulations are given in Table II. According to the simulation results, with the weighting factors become larger, which means more changes for the noise covariance matrices, the filtering divergence is more likely to happen, especially with the suddenly changed acceleration. Besides, the changing measurement noise model

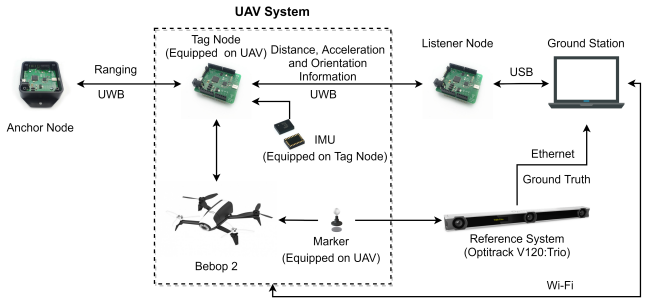

Fig. 4. System components.

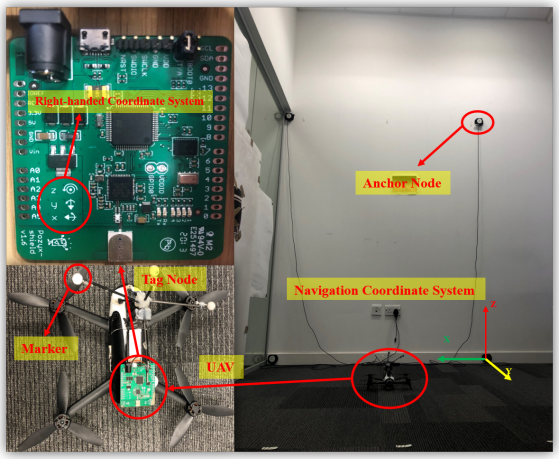

Fig. 5. Experiment environment.

in simulation 2 can also lead to the increasing probability of filtering divergence. For the proposed algorithm, considering the larger weighting factors will only be calculated when the big difference between the observation measurements and the predicted value, or between the recorded average time interval and current time interval is detected. And the calculated weighting factors are all limited within 0.5. Thus, the filtering divergence for the proposed algorithm can be ignored. This can also be proved by the simulation results in Table II.

B. Experiment

1) Experiment environment setup: In order to validate the effectiveness of the proposed algorithm in actual environment, an IMU and UWB based UAV positioning system is developed. The system is consist of five main components shown in Fig. 4, including a commercial micro quadcopter – Parrot Bebop 2, the UWB localisation system (Pozyx) with four anchor nodes, one tag node equipped on Bebop 2 and one listener node, the IMU (BNO-055) attached on UWB tag node, the ground station (laptop) and the OptiTrack V120:Trio to serve as the reference system. In the system, UWB sensor nodes are utilised for distance measurement between the UAV and fixed anchor nodes. The IMU in the system is attached on the UWB tag node to provide the acceleration and orientation information. After the measurement process, the measured distance, acceleration and orientation information will be collected and transmitted by the listener node to the ground station for positioning via USB. Then the position control command will be generated through the estimated position information and the objective points. Finally, the position control command will be transmitted to the Bebop 2 by the ground station through Wi-Fi to achieve the stable flight of UAV. During the process, the ground truth will be provided by the OptiTrack V120:Trio through the localisation of the markers attached on UAV. In the system, in order to keep a stable millimeter-level positioning accuracy, three markers are attached on Bebop 2. The position information of UAV from OptiTrack V120:Trio will be transmitted to the ground station via Ethernet in real-time for the performance evaluation.

In the experiment, in order to evaluate the performance of the proposed algorithm in the specified environment comprehensively, the experiment is performed within a confined space (1.95m $\times$ 3.0m $\times$ 2.3m) in the laboratory to simulate the extremely confined space as depicted in Fig. 5. Similar to the simulation, all anchor nodes in the system are deployed on X-Z plane with the same coordinates to conform the application scenario where is difficult for human to access and the anchor nodes could only be deployed near the entrance of that extremely confined space.

2) UAV Flight Test: Since the propagation condition and operational environment always have a great impact on the positioning performance which may cause the unexpected performance degradation. Two different flight tests have been performed to get rid of this and comprehensively prove the effectiveness of the proposed algorithm under different working conditions. Same as the simulation, in the actual flight tests, the planned trajectory is also set as a reverse "S". The STD for the measurement noise of IMU and UWB sensor nodes in the conventional MLE based TW-TOF approach and the sensor fusion based algorithms are assumed as 0.5m/s^2 and 0.1m which are estimated through 1000 recorded acceleration and distance measurements with UAV at the fixed point and adjusted manually through trial and error.

In the flight test 1, the localisation performance of eight different types of algorithms same as the simulations have been demonstrated and listed in Fig. 6 and Table III. Obviously, the same conclusion compared with the simulation can be made through the localisation results for the flight test 1, that the conventional MLE based TW-TOF algorithm holds the biggest performance oscillation. When being focused on the number of positioning points, with the conventional MLE based TW-TOF algorithm, much more time is required for UAV to hit the target points, which means that this oscillation also results in the instability of UAV. Thus, the results indicate that the measurement noise from the UWB sensor nodes has a great influence on the stability of UAV. However, this oscillation can be greatly limited through the sensor fusion based approaches. As listed in Table III, in contrast with the conventional MLE based TW-TOF algorithm, the performance of other algorithms is all improved significantly, except the algorithm in [17]. However, there is still a great improvement on the 95^{th} percentile error and the average STD of the algorithms in [17] compared with the conventional MLE based TW-TOF.

TABLE III
PERFORMANCE ANALYSIS FOR THE ACTUAL FLIGHT TEST

Flight Test Number	Algorithm	Median Error	Improved	95^{th} Error	Improved	Average STD	Improved
Flight Test 1	MLE based TW-TOF	0.144m	N/A	0.351m	N/A	0.098m	N/A
–	EKF In This Paper	0.116m	19.4%	0.239m	31.9%	0.075m	23.5%
–	[14]	0.129m	10.4%	0.237m	32.5%	0.067m	31.6%
–	[17]	0.149m	-3.5%	0.220m	37.3%	0.053m	45.9%
–	[18]	0.117m	18.8%	0.212m	39.6%	0.054m	44.9%
–	AEKF ($\alpha = \beta = 0.3$)	**0.099m**	**31.3%**	0.199m	43.4%	**0.048m**	**51.0%**
–	AEKF ($\alpha = \beta = 0.5$)	0.107m	25.7%	0.198m	43.6%	0.051m	48.0%
–	**Our Proposed**	0.100m	30.6%	**0.170m**	**51.6%**	0.051m	48.0%
Flight Test 2	EKF In This Paper	0.133m	N/A	0.332m	N/A	0.082m	N/A
–	[14]	0.150m	-12.8%	0.309m	6.9%	0.076m	7.3%
–	[17]	0.122m	8.3%	0.240m	27.7%	0.054m	34.1%
–	[18]	0.148m	-11.3%	0.276m	16.9%	0.068m	17.1%
–	AEKF ($\alpha = \beta = 0.3$)	0.113m	15.0%	0.215m	35.2%	**0.050m**	**39.0%**
–	AEKF ($\alpha = \beta = 0.5$)	0.120m	9.8%	0.227m	31.6%	0.058m	29.3%
–	**Our Proposed**	**0.104m**	**21.8%**	**0.213m**	**35.8%**	0.053m	35.4%

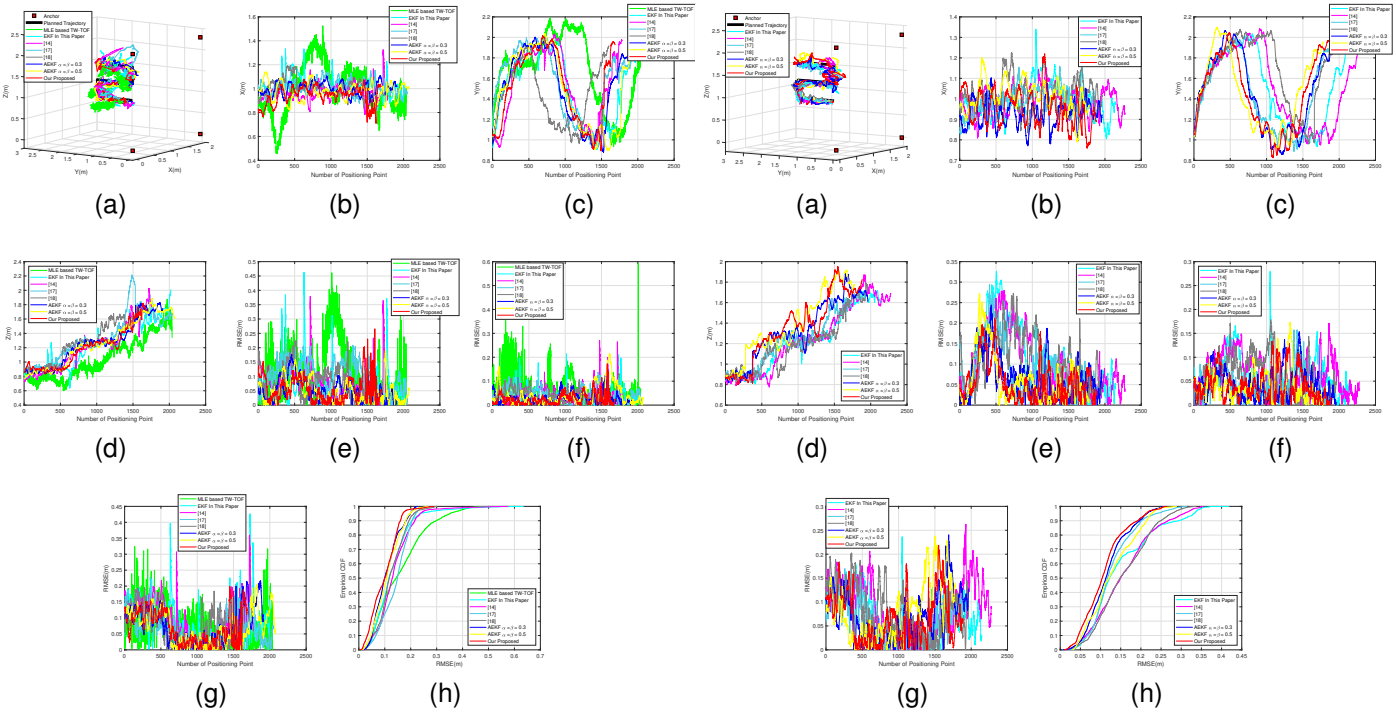

Fig. 6. Flight test results of test 1. (a) 3D trajectories for different algorithms. (b) 3D trajectories in X direction. (c) 3D trajectories in Y direction. (d) 3D trajectories in Z direction. (e) RMSE (m) in X direction. (f) RMSE (m) in Y direction. (g) RMSE (m) of in Z direction. (h) eCDF for different algorithms.

Fig. 7. Flight test results of test 2. (a) 3D trajectories for different algorithms. (b) 3D trajectories in X direction. (c) 3D trajectories in Y direction. (d) 3D trajectories in Z direction. (e) RMSE (m) in X direction. (f) RMSE (m) in Y direction. (g) RMSE (m) in Z direction. (h) eCDF for different algorithms.

When being focused on the sensor fusion based approaches, the EKF algorithm in this paper and the algorithms in [14], [17] and [18] all exploited the manually adjusted and constant noise covariance matrices for positioning. For the EKF algorithm in this paper, it can be observed that a high performance median error (0.116m) can be attained, nevertheless, the 95^{th} percentile error and average STD of the localisation error still keep in high level when compared with the AEKF algorithms. Even the average STD is improved by the additional distance calibration and outlier detection methods in [14] and the 95^{th} percentile error is enhanced by the additional angular rate in [17] and [18], however, a big gap still exists in contrast to the AEKF algorithms, due to the changing environment. For the AEKF algorithms, with the estimated noise covariance matrices $\boldsymbol{R}'_k$ and $\boldsymbol{Q}'_k$, the median error, 95^{th} percentile error and the average STD are all significantly improved with these around 0.102m, 0.189m and 0.05m, respectively. The AEKF algorithm with smaller weighting factors (0.3) holds the best performance on median error and average STD. But there is just a subtle difference for these compared with the proposed algorithm, and the proposed algorithm obtained the best performance on the 95^{th} percentile error (0.170m).

As aforementioned, in order to eliminate the unexpected performance degradation and simulate the variation of the

operational environment, another flight test has been conducted. In this flight test, obstacle is utilised to occlude one of the anchor nodes for a short time period during the flight to simulate the noise changing environment. Considering it is sufficient to prove the effectiveness of the sensor fusion based approaches in contrast with the conventional MLE based TW-TOF on UAV positioning, through the simulations and experiment results from the flight test 1. And to provide much more detailed information. In the flight test 2, only the experiments for the sensor fusion based approaches have been conducted and the results have been provided in Fig. 7 and Table III.

In the flight test 2, the degrading performance can be observed for almost all the algorithms due to the occluded anchor node during the flight test. Especially for the algorithms in [14] and [18], a great performance drop-off can be discovered. This is caused by the unsuitable calibration parameter leaded by the changing measurement noise. For the AEKF algorithms, obviously, in this flight test, the proposed algorithm holds the best performance on the median error (0.104m) and the 95^{th} percentile error (0.213m). Owing to the changing measurement noise, there is a performance degradation for the AEKF algorithm with the smaller weighting factors (0.3). When with smaller weighting factors, more trust will be given to the $\boldsymbol{R}_{offline}$ and $\boldsymbol{Q}_{offline}$ which means more stable performance. However, the system needs more time to catch up the changes, which may result in the accuracy degradation. This can also be proved by the localisation results in the flight test 2, that the median error (0.113m) and the 95^{th} percentile error (0.215m) of the AEKF algorithm with smaller weighting factors (0.3) is worse than the proposed algorithm, but it still holds the best average STD (0.050m).

When combining the experiment results from all the flight tests, the following conclusion can be made that compared with the conventional MLE based TW-TOF algorithm, the EKF algorithm in this paper and the algorithms in [14], [17] and [18], the better performance can be attained by the AEKF algorithms under different conditions. For the comparison within the AEKF algorithms, even the localisation performance for the AEKF based algorithm with constant weighting factors may be better than the proposed algorithm under certain conditions. However, the proposed algorithm always shows much more robust performance, the accuracy and precision always keep in high level with the median error around 0.102m, the 95^{th} percentile error around 0.192m and the average STD around 0.052m. Furthermore, apart from the localisation accuracy and precision, the position update rate also has great influence on the stability of UAV in such environments due to the speed of it. Considering the limitation for the TW-TOF ranging protocol and the propagation speed of the electromagnetic wave, the position update rate for the conventional MLE based TW-TOF algorithm is restrained within 25Hz. This is significantly improved by the sensor fusion approaches which increased the update rate into 88Hz. This high position update rate will absolutely improve the stability of UAV in such environment. In conclusion, it can be proved that the proposed algorithm is capable for UAV applications in focused scenarios.

V. Conclusion

In this article, an AEKF based sensor fusion approach which integrates IMU and UWB focusing on the high precision UAV positioning in extremely confined environments was proposed. Firstly, the overview for the conventional UWB based UAV positioning based approach was presented. Afterwards, the EKF based sensor fusion approach was introduced to remedy the existing issues. However, considering the unknown process and measurement noise covariance matrices, the performance oscillation still exists, and the precision and accuracy are insufficient for the stable flight of UAV in extreme cases. Therefore, the AEKF based sensor fusion approach was studied and proposed. With the measurements from previous processes, the process and measurement noise covariance matrices can be adaptively estimated to relieve the performance oscillation. During the estimation process, two weighting factors α and β were introduced and adaptively estimated through the recorded information to further limit the estimation of these matrices for performance improvement. Finally, simulations and experiments have been carried out to comprehensively evaluate the performance. From results, it is clear that, in contrast with the conventional MLE based TW-TOF localisation algorithm, the EKF based approach in this paper, the algorithms in [14], [17] and [18], and the AEKF based approach with constant weighting factors, the proposed algorithm can always show better and robust performance with the median positioning error around 0.102m, 95^{th} percentile positioning error around 0.192m and average STD around 0.052m. The position update rate is also increased to 88Hz which can absolutely improve the stability of the UAV in the focused environment. Accordingly, the proposed algorithm and system are suitable for UAV applications in focused scenarios.

Acknowledgments

The authors would like to thank the Net Zero Technology Centre robotics team at the University of Strathclyde for their kindly support especially Dr Gordon Dobie, Dr Charles MacLeod, Mr Mark Robertson and Prof Xiutian Yan.

References

[1] P. Petráček, V. Krátkỳ, and M. Saska, "Dronument: System for reliable deployment of micro aerial vehicles in dark areas of large historical monuments," *IEEE Robot. Autom. Lett.*, vol. 5, no. 2, pp. 2078–2085, 2020.

[2] T. Özaslan, G. Loianno, J. Keller, C. J. Taylor, and V. Kumar, "Spatio-temporally smooth local mapping and state estimation inside generalized cylinders with micro aerial vehicles," *IEEE Robot. Autom. Lett.*, vol. 3, no. 4, pp. 4209–4216, 2018.

[3] P. De Petris, H. Nguyen, M. Kulkarni, F. Mascarich, and K. Alexis, "Resilient collision-tolerant navigation in confined environments," in *Proc. IEEE Int. Conf. Robot. Automat.* IEEE, 2021, pp. 2286–2292.

[4] P. De Petris, H. Nguyen, T. Dang, F. Mascarich, and K. Alexis, "Collision-tolerant autonomous navigation through manhole-sized confined environments," in *Proc. IEEE Int. Symp. Safety, Secur., Rescue Robot.* IEEE, 2020, pp. 84–89.

[5] M. Petrlík, T. Báča, D. Heřt, M. Vrba, T. Krajník, and M. Saska, "A robust uav system for operations in a constrained environment," *IEEE Robot. Autom. Lett.*, vol. 5, no. 2, pp. 2169–2176, 2020.

[6] P. Tripicchio, M. Satler, M. Unetti, and C. A. Avizzano, "Confined spaces industrial inspection with micro aerial vehicles and laser range finder localization," *Int. J. Micro Air Vehicles*, vol. 10, no. 2, pp. 207–224, 2018.

[7] R. Liu, Y. He, C. Yuen, B. P. L. Lau, R. Ali, W. Fu, and Z. Cao, "Cost-effective mapping of mobile robot based on the fusion of uwb and short-range 2-d lidar," *IEEE/ASME Trans. Mechatronics*, vol. 27, no. 3, pp. 1321–1331, 2022, doi: 10.1109/TMECH.2021.3087957.

[8] R. Y. Brogaard, M. Zajaczkowski, L. Kovac, O. Ravn, and E. Boukas, "Towards uav-based absolute hierarchical localization in confined spaces," in *Proc. IEEE Int. Symp. Safety, Secur., Rescue Robot.* IEEE, 2020, pp. 182–188.

[9] J. Qian, K. Chen, Q. Chen, Y. Yang, J. Zhang, and S. Chen, "Robust visual-lidar simultaneous localization and mapping system for uav," *IEEE Geosci. Remote Sens. Lett.*, vol. 19, pp. 1–5, 2021.

[10] D. Kang and Y.-J. Cha, "Autonomous uavs for structural health monitoring using deep learning and an ultrasonic beacon system with geo-tagging," *Comput.-Aided Civil Infrastructure Eng.*, vol. 33, no. 10, pp. 885–902, 2018.

[11] S. Kuutti, S. Fallah, K. Katsaros, M. Dianati, F. Mccullough, and A. Mouzakitis, "A survey of the state-of-the-art localization techniques and their potentials for autonomous vehicle applications," *IEEE Internet Things J.*, vol. 5, no. 2, pp. 829–846, 2018.

[12] B. Yang and E. Yang, "A survey on radio frequency based precise localisation technology for uav in gps-denied environment," *J. Intell. Robot. Syst.*, vol. 103, no. 3, pp. 1–30, 2021.

[13] A. Benini, A. Mancini, and S. Longhi, "An imu/uwb/vision-based extended kalman filter for mini-uav localization in indoor environment using 802.15. 4a wireless sensor network," *J. Intell. Robot. Syst.*, vol. 70, no. 1, pp. 461–476, 2013.

[14] K. Guo, Z. Qiu, C. Miao, A. H. Zaini, C.-L. Chen, W. Meng, and L. Xie, "Ultra-wideband-based localization for quadcopter navigation," *Unmanned Syst.*, vol. 4, no. 01, pp. 23–34, 2016.

[15] J. Li, Y. Bi, K. Li, K. Wang, F. Lin, and B. M. Chen, "Accurate 3d localization for mav swarms by uwb and imu fusion," in *Proc. 14th IEEE Int. Conf. Control Autom.* IEEE, 2018, pp. 100–105.

[16] D. Feng, C. Wang, C. He, Y. Zhuang, and X.-G. Xia, "Kalman-filter-based integration of imu and uwb for high-accuracy indoor positioning and navigation," *IEEE Internet Things J.*, vol. 7, no. 4, pp. 3133–3146, 2020.

[17] M. Strohmeier, T. Walter, J. Rothe, and S. Montenegro, "Ultra-wideband based pose estimation for small unmanned aerial vehicles," *IEEE Access*, vol. 6, pp. 57 526–57 535, 2018.

[18] M.-G. Li, H. Zhu, S.-Z. You, and C.-Q. Tang, "Uwb-based localization system aided with inertial sensor for underground coal mine applications," *IEEE Sensors Journal*, vol. 20, no. 12, pp. 6652–6669, 2020.

[19] M. Song, R. Astroza, H. Ebrahimian, B. Moaveni, and C. Papadimitriou, "Adaptive kalman filters for nonlinear finite element model updating," *Mech. Syst. Signal Process.*, vol. 143, p. 106837, 2020.

[20] Y. Huang, Y. Zhang, B. Xu, Z. Wu, and J. A. Chambers, "A new adaptive extended kalman filter for cooperative localization," *IEEE Trans. Aerosp. Electron. Syst.*, vol. 54, no. 1, pp. 353–368, 2017.

[21] Y. Huang, M. Bai, Y. Li, Y. Zhang, and J. Chambers, "An improved variational adaptive kalman filter for cooperative localization," *IEEE Sensors J.*, vol. 21, no. 9, pp. 10 775–10 786, 2021.

[22] F. Jiancheng and Y. Sheng, "Study on innovation adaptive ekf for in-flight alignment of airborne pos," *IEEE Trans. Instrum. Meas.*, vol. 60, no. 4, pp. 1378–1388, 2011.

[23] F. Lazzari, A. Buffi, P. Nepa, and S. Lazzari, "Numerical investigation of an uwb localization technique for unmanned aerial vehicles in outdoor scenarios," *IEEE Sensors J.*, vol. 17, no. 9, pp. 2896–2903, 2017.

[24] Z. Shi, H. Li, H. Lin, and L. Huang, "A nano-quadcopter formation flight system based on uwb indoor positioning technology," in *Proc. 13th Int. Conf. Comput. Sci. Edu.* IEEE, 2018, pp. 1–4.

[25] K. Guo, X. Li, and L. Xie, "Ultra-wideband and odometry-based cooperative relative localization with application to multi-uav formation control," *IEEE Trans. Cybern.*, vol. 50, no. 6, pp. 2590–2603, 2019.

[26] B. Yang, E. Yang, L. Yu, and A. Loeliger, "High-precision uwb-based localisation for uav in extremely confined environments," *IEEE Sensors J.*, vol. 22, no. 1, pp. 1020–1029, 2021.

[27] J. Kelly and G. S. Sukhatme, "Visual-inertial sensor fusion: Localization, mapping and sensor-to-sensor self-calibration," *Int. J. Robot. Res.*, vol. 30, no. 1, pp. 56–79, 2011.

[28] S. Akhlaghi, N. Zhou, and Z. Huang, "Adaptive adjustment of noise covariance in kalman filter for dynamic state estimation," in *Proc. IEEE Power Energy Soc. Gen. Meeting*. IEEE, 2017, pp. 1–5.

[29] Gazebo. Gazebo online tutorial. [Online]. Available: https://gazebosim.org

Beiya Yang (IEEE Graduate Student Member, 2019) received the B.Eng. degree in Electronic Information Engineering from Northwestern Polytechnical University, Xi'an, China, in 2013 and the M.Sc degree in Information and Communication Engineering from National University of Defense Technology, Changsha, China, in 2015. He is currently pursuing the Ph.D. degree in the Department of Design, Manufacturing and Engineering Management (DMEM) at University of Strathclyde, Glasgow, UK, since 2019. His current research interests include indoor localisation technology, unmanned aerial vehicles (UAV) localisation and wireless sensor networks.

Erfu Yang (IEEE Senior Member, 2022) received his Ph.D. degree in Robotics from the School of Computer Science and Electronic Engineering, University of Essex, Colchester, UK, in 2008. He is currently a Senior Lecturer in the Department of Design, Manufacturing and Engineering Management (DMEM), University of Strathclyde, Glasgow, UK. His main research interests include robotics, autonomous systems, mechatronics, manufacturing automation, signal and image processing, computer vision and applications of machine learning and artificial intelligence, etc. He has over 160 publications in these areas, including more than 80 journal papers and 10 book chapters. Dr. Yang has been awarded over 15 research grants as PI (principal investigator) or CI (co-investigator). He is the Fellow of the UK Higher Education Academy, Member of the UK Engineering Professors' Council, Senior Member of the IEEE Society of Robotics and Automation, IEEE Control Systems Society, Publicity Co-Chair of the IEEE UK and Ireland Industry Applications Chapter, Committee Member of the IET SCOTLAND Manufacturing Technical Network. He is also an associate editor for the Cognitive Computation journal published by Springer.

Leijian Yu received the B.Eng. degree in electrical information engineering and the M.Sc degree in information and communication engineering from China University of Petroleum (East China), Qingdao, China, in 2015 and 2018, respectively. He is currently pursuing the Ph.D. degree in the Department of Design, Manufacturing and Engineering Management (DMEM) at the University of Strathclyde, Glasgow, UK, since 2018. His current research interests include machine learning with applications on unmanned aerial vehicles (UAV), UAV vision-based autonomous navigation and image contrast enhancement.

Cong Niu (IEEE Member, 2021) has been awarded the B.Eng. with Honours, degree of Electronic Engineering from University of Central Lancashire, Preston, UK in 2014. Then awarded with the M.Sc degree on Embedded Digital System from University of Sussex, Brighton, UK in 2015. He received his Ph.D. degree in the Department of Design, Manufacturing and Engineering Management (DMEM), University of Strathclyde, Glasgow, UK, in 2021. He is currently working as a Research Associate in DMEM. His current research interests include field and indoor path planning, modeling and simulation, unmanned ground and aerial vehicles and smart factory.